14th International Symposium on Turbulence and Shear Flow Phenomena (TSFP14)
Heidelberg, Germany, July 28-31, 2026

A MULTI-PARAMETER CORRELATION FOR THE ROUGHNESS FUNCTION IN TURBULENT PIPE AND CHANNEL FLOW

A. Sojoudi
Department of Mechanical Engineering,
College of Engineering,
University of Saskatchewan, Canada
ats858@usask.ca

D. J. Bergstrom
Department of Mechanical Engineering,
College of Engineering,
University of Saskatchewan, Canada
don.bergstrom@usask.ca

ABSTRACT

The prediction of drag in turbulent flows over rough surfaces remains a central challenge, particularly for irregular geometries where classical equivalent sand-grain scaling is limited and does not achieve universal applicability. In this study, a multi-parameter correlation for the roughness function, ΔU^{+}, is developed using a comprehensive database of 172 direct numerical simulation (DNS) and large eddy simulation (LES) cases spanning regular, irregular, and engineered roughness in both pipe and channel flows. Building on a systematic evaluation of morphological descriptors, the proposed formulation incorporates logarithmic scaling in the root-mean-square roughness height (k_{rms}^{+}), nonlinear dependence on effective slope (ES), and a linear contribution of skewness (Sk), together with interaction terms that capture the coupled influence of amplitude and geometry. The predictive capability of the proposed correlation is assessed by comparison with independent DNS datasets that were not used in the training process. To demonstrate practical applicability, the proposed roughness function is further employed to estimate the friction factor (f) in fully developed internal flows. By using the predicted ΔU^{+}, friction factor is obtained without invoking equivalent sand-grain roughness. The results show that the present formulation provides consistent predictions of both flow quantities (ΔU^{+} and f) across a wide range of surface morphologies. These findings support the use of morphology-based correlations as a practical alternative to traditional parameterizations, particularly in the transitionally rough regime.

INTRODUCTION

Surface roughness affects wall-bounded turbulence across aerospace, marine, energy, and environmental systems. Real surfaces rarely remain smooth; erosion, corrosion, deposition, and fouling introduce multiscale roughness that penetrates the near-wall region and modifies turbulence dynamics. The presence of roughness increases skin-friction drag, alters coherent structures, and produces a downward shift in the logarithmic portion of the mean velocity profile. This shift, known as the roughness function, quantifies the additional drag penalty relative to a smooth wall and serves as a key input for friction factor prediction and near-wall modeling in Reynolds-Averaged Navier-Stokes (RANS) and wall-modeled LES. Even micron-scale roughness can perturb high-Reynolds-number flows, leading to measurable efficiency losses in compressors, pipelines, and marine vessels, and contributing to increased energy consumption and emissions in engineering systems (Chung et al., 2021).

The systematic study of roughness effects began with the classical experiments of Nikuradse (1933), who established the relationship between roughness and wall shear stress using sand-grain surfaces. Schlichting (1936) introduced the concept of equivalent sand-grain roughness height k_s, providing a framework for relating arbitrary surfaces to a canonical roughness scale. This concept was later incorporated into the Colebrook–White (1937) relation and the Moody (1944) diagram, forming the basis for engineering predictions of friction factor across smooth, transitional, and fully rough regimes. While this approach remains widely used, it relies on the inference of k_s from emperical tables, making it inherently indirect. This limitation becomes particularly significant for irregular, multiscale surfaces, where small uncertainties in ΔU^{+} can lead to large errors in k_s^{+}, especially in the transitionally rough regime where both viscous and pressure drag mechanisms coexist (Chung et al., 2021; Flack & Schultz, 2014).

As noted above, rough-wall flows are commonly categorized into hydraulically smooth, transitionally rough, and fully rough regimes. In the smooth regime, roughness elements remain submerged within the viscous sublayer and have negligible influence on turbulence. In the fully rough regime, viscous effects vanish and drag is dominated by pressure forces acting on the roughness elements, leading to a Reynolds number–independent shift in the velocity profile. The transitionally rough regime remains the most challenging to model, as it involves a complex interplay between viscous stresses, form drag, and turbulence production. In this regime, the drag response is highly sensitive to surface morphology, and classical scaling based on a single roughness height often becomes insufficient to collapse experimental or numerical data.

To address these limitations, recent research has shifted toward describing roughness in terms of geometric and statistical descriptors that directly characterize surface morphology. These include the mean absolute height k_a^{+}, root-mean-square height k_{rms}^{+}, effective slope ES, skewness Sk, and kurtosis Ku, which together encode the amplitude, steepness, and asymmetry of the surface. Advances in surface scanning and digital reconstruction have made these parameters accessible for both experimental and numerical studies. Among these descriptors, effective slope has emerged as a key parameter governing pressure drag, as it represents the exposure of roughness elements to the incoming flow. Studies have shown that ΔU^{+} increases rapidly with ES up to a critical threshold (approximately $ES \approx 0.35$), beyond which mutual sheltering between roughness elements reduces the sensitivity of drag to further increases in slope (Napoli et al., 2008; Schultz & Flack, 2010).

In addition to slope, the asymmetry of the surface plays a crucial role. Positive skewness, corresponding to peak dominated surfaces, enhances form drag by promoting flow separation and strong pressure gradients at crests, while negative skewness, associated with valley-dominated surfaces, can shield the flow and reduce momentum exchange. This asymmetry has been shown to produce different turbulence responses (Flack et al., 2020). Furthermore, interactions between amplitude and slope, as well as higher-order statistical features, have been shown to influence drag, indicating that the underlying physics of rough-wall turbulence is inherently multi-parameter and nonlinear.

Despite these advances, most existing correlations remain limited in scope. Many are developed for specific roughness families, such as sinusoidal or packed-element surfaces, or rely on hydrodynamic parameters such as k_s, which restricts their predictive generality. Even more recent formulations that incorporate multiple descriptors often remain calibrated to relatively small datasets, making their applicability to diverse, irregular surfaces uncertain. As a result, a unified, geometry-based framework capable of predicting ΔU^+ across both regular and irregular surfaces, particularly in the transitionally rough regime, remains an open challenge.

In this work, we address this gap by compiling a database of 172 data points from 16 DNS studies, including a wide range of Reynolds numbers, roughness morphologies, and flow configurations in pipes and channels. Building on a systematic regression framework, we identify physically relevant descriptors and their interactions, including logarithmic and nonlinear dependence on k_{rms}^+, quadratic contributions of ES, cross-interaction terms, linear skewness effects, and a weak dependence on k_a^+. These terms are consolidated into a single predictive expression that captures the combined effects of amplitude, slope, and asymmetry. Furthermore, the formulation enables direct prediction of ΔU^+ and f from surface morphology without invoking the equivalent sand-grain roughness k_s, providing a practical alternative for engineering modeling of rough-wall turbulence.

DATA COMPILATION

A comprehensive database of 172 data points was assembled from sixteen high-fidelity DNS and LES studies of turbulent flow over rough walls, spanning both pipe and channel configurations (Table 1). The dataset includes friction Reynolds numbers up to $Re_\tau \approx 1000$, and covers both transitionally rough and fully rough regimes. This broad parameter space enables an assessment of the roughness function across diverse flow conditions and surface morphologies.

The database includes canonical periodic roughness, realistic scanned surfaces, and statistically generated irregular geometries. Canonical configurations, such as sinusoidal roughness in pipe flow (Chan et al., 2015; 2018), provide well-controlled benchmark cases where geometric parameters can be systematically varied and directly linked to roughness effects. These serve as reference cases for understanding the fundamental behavior of rough-wall turbulence.

To complement these idealized surfaces, the database incorporates a wide range of realistic and industrially relevant roughness geometries. These include grit-blasted and graphite surfaces (Busse, Thakkar & Sandham, 2017), as well as scanned engineering surfaces representative of manufacturing and operational conditions (De Maio et al., 2023). Such datasets capture the complexity of real-world roughness, where erosion, corrosion, and deposition processes generate highly irregular and multiscale topographies that cannot be represented by simple geometric parameters.

A major portion of the database consists of statistically generated rough surfaces, where morphology is defined through controlled variation of key descriptors such as effective slope, skewness, and roughness height. These datasets (e.g., Yuan & Piomelli, 2014; De Marchis et al., 2020; Kuwata & Kawaguchi, 2019; Jouybari et al., 2021; Yang et al., 2022) are particularly valuable because they enable systematic isolation of individual geometric effects while maintaining physically realistic surface structures. They include both random and multi-scale roughness, as well as anisotropic configurations, allowing for a detailed investigation of how different morphological features influence drag generation.

The database further includes specialized roughness types that extend its applicability. Additively manufactured surfaces (Garg et al., 2023) provide insight into emerging engineering materials with complex surface textures, while biologically inspired roughness such as barnacle-type configurations (Sarakinos & Busse, 2022) captures the effects of marine biofouling. Additionally, datasets focusing on higher-order statistical variations, including skewness and kurtosis (Busse & Jelly, 2023), enable the assessment of asymmetry and intermittency effects in rough-wall turbulence. Together, these contributions ensure that the database spans both controlled parametric studies and realistic engineering surfaces.

To ensure consistency and focus on canonical rough-wall behavior, a set of filtering criteria was applied to the compiled dataset. Highly dense roughness configurations, where the dominant length scale becomes gap-based and canopy-flow dynamics prevail, were excluded. Strongly anisotropic surfaces, which introduce directional alignment effects beyond the scope of the present model, were also removed. In addition, cases with incomplete velocity profile information (insufficient for reliable extraction of ΔU^+) or missing topographic statistics were discarded. These exclusions ensure that the remaining dataset is both physically consistent and suitable for regression analysis.

After applying these filters, the final database retains 172 high-quality data points, covering $Re_\tau = 90$–1000, $k_a^+ = 2.0$–71.2, $k_{rms}^+ = 2.5$–60.0, $ES = 0.06$–1.13, and $Sk = -2.3$–4.06. This range reflects a broad spectrum of roughness morphologies and flow conditions, providing a foundation for the development and validation of the proposed correlation.

SYSTEMATIC DEVELOPMENT OF THE CORRELATION

The proposed correlation is not introduced as an arbitrary functional form but rather developed through a systematic assessment of how individual roughness descriptors and their interactions influence the roughness function. The formulation follows a progressive strategy, beginning with single-parameter representations and incrementally incorporating additional terms based on both statistical improvement and physical reasoning. The analysis initially considers the effective slope (ES). However, when used alone, ES exhibits limited predictive capability. Linear scaling fails to represent the observed behavior, whereas a nonlinear form better captures the rapid increase in drag at low slopes followed by a gradual saturation at higher values. This trend reflects the physical mechanism whereby increasing steepness promotes flow separation, while further increases lead to wake interactions and sheltering effects that constrain additional drag growth.

To account for roughness amplitude, the root-mean-square height k^+_{rms} is introduced. A logarithmic dependence on k^+_{rms} improves the prediction of ΔU^+, reflecting the diminishing sensitivity of drag to height as roughness elements become large relative to the viscous scale. More importantly, combining k^+_{rms} with ES through interaction terms reduces prediction error, indicating that drag depends not only on roughness size but also on its exposure to the flow. The inclusion of mean roughness height k^+_a provides only marginal improvement, suggesting that k^+_{rms} captures the dominant amplitude effects. Finally, skewness (Sk) is incorporated to account for surface asymmetry. A linear skewness term enhances predictive accuracy by distinguishing between peak and valley-dominated geometries.

The present model is inspired by these logarithmic and mixed-parameter formulations, but extends them by systematically incorporating additional interaction terms identified through the regression analysis. In particular, the inclusion of nonlinear contributions in both k^+_{rms} and ES, as well as cross-interaction terms and a linear skewness component, allows the model to capture the coupled effects of amplitude, slope, and asymmetry within a single framework. Based on this development, the proposed correlation takes the following generalized form:

$$\begin{aligned}\Delta U^+ = A_1 + A_2\, lnk^+_{rms} + A_3(lnk^+_{rms})^2 \\ + A_4 ES + A_5 ES^2 \\ + A_6 ES(lnk^+_{rms}) \\ + A_7 Sk \\ + A_8 ln(ESk^+_{rms}) \\ + A_9[ln(ESk^+_{rms})]^2 \\ + A_{10}(lnk^+_a)\end{aligned} \quad (1)$$

where A_i are regression coefficients determined from the compiled database. The coefficients obtained from the regression analysis are A_1=7.33, A_2=1.47, A_3=-0.69, A_4=-8.07, A_5=10.58, A_6=-7.56, A_7=0.68, A_8=-5.19, A_9=1.02, and A_{10}=-0.52, yielding a coefficient of determination of $R^2 \approx 0.95$ for the compiled dataset.

RESULTS

The performance of the proposed correlation is evaluated using both global and local statistical measures, with emphasis on its ability to reproduce the roughness function across a wide range of surface morphologies and flow conditions. In addition to the coefficient of determination, the analysis considers the distribution of prediction errors to assess model bias. The results are presented in four parts: comparison with the training dataset, analysis of residual distributions, validation against independent datasets, and application to friction factor prediction.

Figure 1 presents a comparison between the predicted roughness function ΔU^+_{pred} and DNS values ΔU^+_{DNS} for the compiled database. The predictions from the present model are shown alongside those from the correlation of Bornhoft et al. (2023), providing a direct benchmark against a recent multi-parameter formulation. The data collapse around the 1:1 line, with the majority of points falling within the ±5% error bounds. Compared to the reference model, the present correlation exhibits a tighter clustering and reduced scatter, particularly in the intermediate range of ΔU^+, which corresponds primarily to the transitionally rough regime. This indicates that the inclusion of nonlinear and interaction terms between k^+_{rms}, ES, and Sk improves the model's ability to capture the coupled mechanisms governing drag generation.

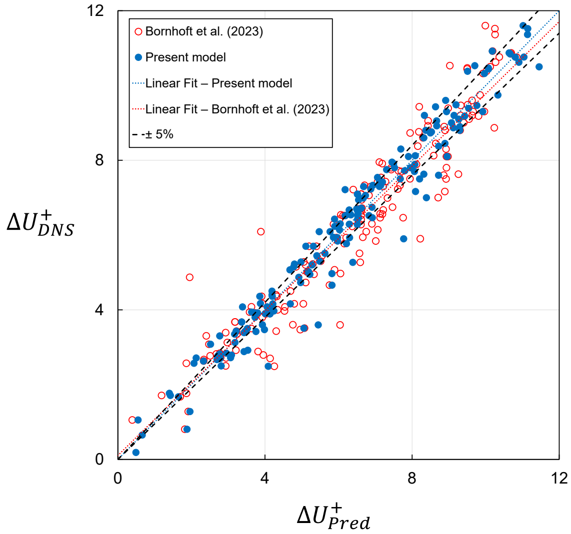

Figure 1. Comparison of predicted roughness function ΔU^+_{Pred} from the present regression model (filled markers) and the correlation of Bornhoft et al. (2023) (open markers) against DNS data, ΔU^+_{DNS}.

While Figure 1 provides a global assessment of predictive accuracy, further insight is obtained by examining the probability density function (PDF) of the residuals, defined as $\Delta U^+_{\text{pred}} - \Delta U^+_{\text{DNS}}$, as shown in Figure 2. The residual distribution for the present model is sharply peaked, indicating a high concentration of predictions near the DNS values. However, the peak is slightly shifted toward negative values, revealing a mild tendency to underpredict ΔU^+ for a subset of cases. In addition, the presence of a secondary peak and asymmetry in the distribution suggests that the model does not capture all variability uniformly across the dataset, particularly for certain surface morphologies.

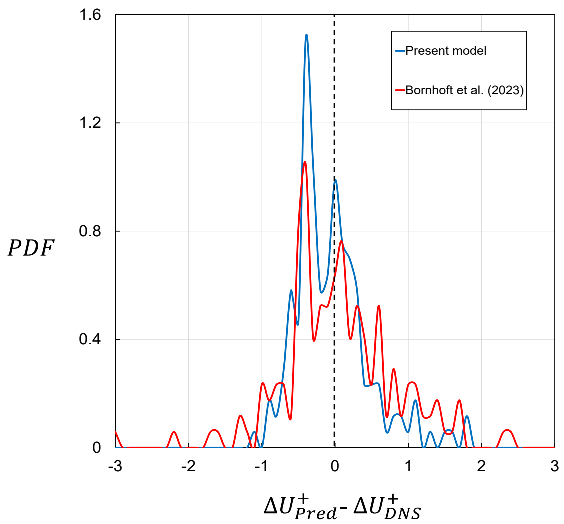

Figure 2. Probability density function (PDF) of residuals between predicted and DNS ΔU^+ for the present model (blue) and the correlation of Bornhoft et al. (2023) (red).

Compared to the correlation of Bornhoft et al. (2023), which exhibits a broader distribution and longer tails, the present model shows reduced overall scatter. Nevertheless, both models display non-negligible deviations from perfect symmetry. The remaining spread in the residuals likely reflects unresolved influences of higher-order geometric features or flow-dependent effects that are not fully captured by the selected descriptors. Despite these limitations, the narrower central distribution associated with the present model indicates improved consistency across the dataset, particularly within the transitionally rough regime where variability is typically largest.

To assess the generality of the proposed correlation, three independent datasets, not included in the regression process, are compiled and used for validation. These datasets, total 32 DNS datapoints, include a broad range of roughness geometries and flow conditions, including statistically generated Gaussian rough surfaces (Bruno et al., 2024), realistic engineering roughness derived from combustion chamber deposits (Forooghi et al., 2018), and canonical sinusoidal roughness configurations with systematic variation of Reynolds number (Ma et al., 2022). Across these studies, turbulent channel flows are considered with friction Reynolds numbers spanning approximately $Re_\tau = 180$ to 1080. The associated roughness metrics include k_{rms}^+ values from approximately 0.8 to 30, effective slope ES ranging from about 0.08 to 1.46, and skewness Sk varying from near-zero values for symmetric sinusoidal surfaces to positive values (up to $Sk \approx 3$). The Gaussian-based surfaces provide controlled variation of amplitude, slope, and asymmetry, while the deposit-based surfaces introduce multi-scale, heterogeneous geometries representative of industrial roughness. In addition to validating the prediction of the roughness function, the same datasets are subsequently employed to assess the applicability of the model in predicting friction factor, thereby linking local roughness effects to global flow resistance.

Figure 3 evaluates the performance of the proposed correlation by directly comparing predicted values of ΔU^+ against corresponding reference data obtained from the compiled DNS dataset. The inclusion of the ±10% bounds provides a quantitative measure of prediction accuracy. The majority of the data points fall within this band, demonstrating that the proposed formulation maintains a consistent reliability across different roughness geometries and flow regimes.

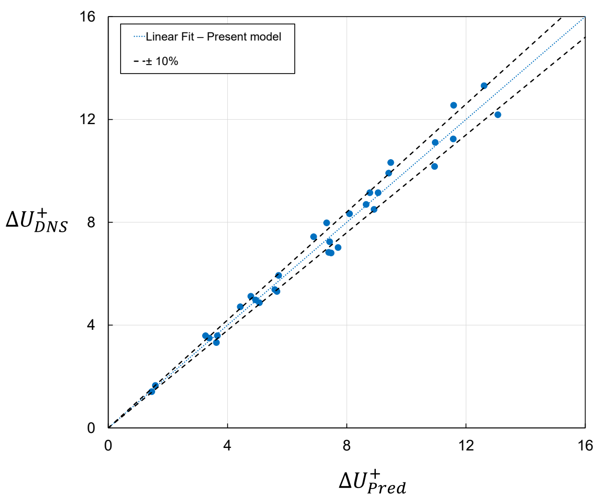

Figure 3. Comparison between predicted and DNS values of the roughness function using the present correlation. The dotted line represents a 1:1 dependence, while the dashed lines indicate a ±10% deviation band.

To evaluate the predictive capability of the proposed correlation in terms of engineering quantities, the roughness function is converted into friction factor. This is achieved by relating the roughness function to the difference between smooth and rough-wall velocity scales through

$$\Delta U^+ = \sqrt{\frac{8}{f}}_s - \sqrt{\frac{8}{f}}_r \qquad (2)$$

where subscripts s and r denote smooth and rough conditions, respectively. For a given roughness condition, ΔU^+ is obtained from Equation 1. The smooth-wall friction factor is evaluated independently by integrating the logarithmic law of the wall over the full channel height to obtain the bulk velocity.

Figure 4 presents an assessment of the proposed framework in predicting the friction factor based on the estimated roughness function. The comparison shows an agreement between predicted and reference values across the range of flow conditions considered. Data points fall within the ±15% error bounds.

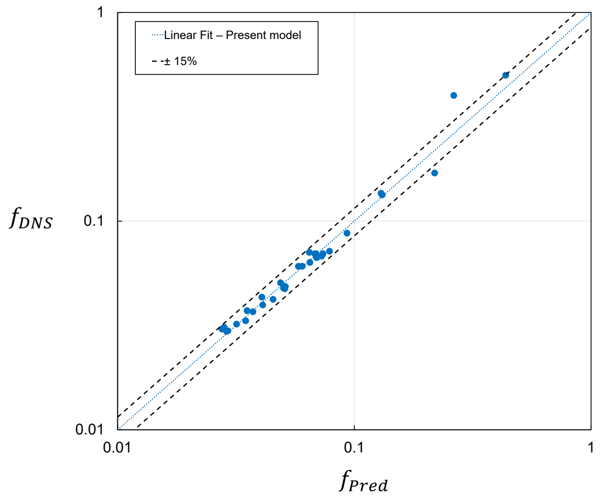

Figure 4. Comparison between predicted and reference friction factor values obtained using the present roughness-function-based framework. The solid line represents a linear fit, while the dashed lines indicate a ±15% deviation band.

CONCLUSION

A correlation for the roughness function has been developed through a stepwise evaluation of key roughness descriptors and their interactions. The analysis shows that effective slope (ES) captures the primary trend associated with pressure drag, but its predictive capability remains limited when used alone. Introducing a nonlinear dependence on ES improves the representation, particularly by capturing the observed saturation behavior at higher slopes. The incorporation of roughness amplitude through k_{rms}^+, using a logarithmic scaling, leads to a noticeable improvement in agreement with reference data, reflecting the reduced sensitivity of drag to height at larger roughness scales. More importantly, combining k_{rms}^+ with ES through interaction terms provides reduction in prediction error, indicating that drag generation depends on both the magnitude of roughness and its effective exposure to the flow. The final formulation, including skewness (Sk), yields a coefficient of determination $R^2 \approx 0.95$, with most predictions of ΔU^+ falling within a ±10% deviation band for an independent dataset of 32 DNS studies. When extended to friction factor prediction using the relation between ΔU^+ and friction factor, and a smooth-channel friction factor obtained from log-law integration, the results remain within approximately ±15% of the reference values across the range of Reynolds numbers and roughness conditions considered. These levels of agreement suggest that the selected descriptors can capture the dominant patterns governing rough-wall flow resistance. Future work will focus on refining the role of skewness by introducing regime-mechanism dependent correlations based on its sign. In particular, distinguishing between peak-dominated and valley-dominated surfaces is expected to improve the representation of asymmetric roughness effects, especially in transitional rough regimes.

Table 1. Details of the constructed DNS database (PF: Pipe Flow, CH: Channel Flow).

Paper	Cases	Re_τ	k_a^+	k_{rms}^+	ES	Sk	Flow
Chan et al. (2018)	8	540	8.1 – 32.0	10.0 – 40.0	0.18 – 0.72	0	PF
Yuan & Piomelli (2014)	17	400 - 1000	8.0 – 67.8	2.6 – 30.2	0.08 – 0.38	-0.02 – 0.46	CF
Busse, Thakkar & Sandham (2017)	14	90 - 720	2.4 – 20.8	3.2 - 26.6	0.23 - 0.28	-0.52 - 0.28	CF
De Marchis et al. (2020)	5	180 - 1000	9.0 – 50.0	10.6 – 60.0	0.10 – 0.2	-0.30 – 0.01	CF
Thakkar, Busse & Sandham (2017)	17	180	4.3 – 7.4	5.7 - 9.1	0.06 - 0.31	-0.52 - 0.59	CF
Kuwata & Kawaguchi (2019)	5	600	13.2 – 39.0	20.1 – 20.8	0.31 – 0.52	-1.00 – 1.00	CF
Jouybari et al. (2021)	29	1000	9.0 – 65.0	8.0 – 33.0	0.07 – 1.13	-0.53 - 2.37	CF
Kuwata & Nagura (2020)	7	600	6.7	8.4	0.10 – 0.60	-0.53 – 0.53	CF
Busse & Jelly (2020)	9	395	8.3 – 9.8	10.6 – 12.6	0.10 – 0.45	-0.07 – 0.07	CF
De Maio et al. (2023)	8	123 - 570	3.8 – 24.5	4.9 – 25.7	0.23 - 0.28	-0.52 - 0.28	PF
Forooghi et al. (2018)	9	450 - 480	22.5 – 71.2	20.4 - 21.7	0.60 - 0.88	-0.35 - 0.67	CF
Chan et al. (2015)	17	180 - 540	2.0 – 32.4	2.5 – 40.0	0.13 - 0.36	0	PF
Garg et al. (2023)	3	450 - 875	5.3 – 23.6	9.4 – 41.7	0.10 – 0.21	0.60	PF
Sarakinos & Busse (2022)	5	395	3.5 – 11.5	7.1 – 13.5	0.07 – 0.40	0.88 – 4.06	CF
Busse & Jelly (2023)	7	395	6.6 – 10.3	9.2 – 13.0	0.20	-2.30 – 2.30	CF
Yang et al. (2022)	12	500	23.0 – 37.0	10.0 – 10.4	0.37 – 0.57	-0.48 – 0.48	CF
Total	**172**	**90 - 1000**	**2.0 – 71.2**	**2.5 – 60.0**	**0.06 – 1.13**	**-2.3 – 4.06**	

REFERENCES

Bornhoft, B., Jain, S. S., and Moin, P., 2023, “A Velocity Transformation for Rough-Wall-Bounded Turbulent Flows,” *Annual Research Briefs*, Center for Turbulence Research, Stanford University, pp. 1–12.

Bruno, F., De Marchis, M., and Napoli, E., 2024, “The Role of the Areal Parameters on Turbulent Flow over 2D Gaussian Roughness,” *International Journal of Heat and Fluid Flow*, Vol. 106, 109287.

Busse, A., Thakkar, M., and Sandham, N. D., 2017, “Reynolds-Number Dependence of the Near-Wall Flow over Irregular Rough Surfaces,” *Journal of Fluid Mechanics*, Vol. 810, pp. 196–224.

Busse, A., and Jelly, T. O., 2023, “Effect of High Skewness and Kurtosis on Turbulent Channel Flow over Irregular Rough Walls,” *Journal of Turbulence*, Vol. 24, No. 1–2, pp. 57–81.

Chan, L., MacDonald, M., Chung, D., Hutchins, N., and Ooi, A., 2015, “A Systematic Investigation of Roughness Height and Wavelength in Turbulent Pipe Flow in the Transitionally Rough Regime,” *Journal of Fluid Mechanics*, Vol. 771, pp. 743–777.

Chan, L., MacDonald, M., Chung, D., Hutchins, N., and Ooi, A., 2018, “Secondary Motion in Turbulent Pipe Flow with Three-Dimensional Roughness,” *Journal of Fluid Mechanics*, Vol. 854, pp. 5–33.

Chung, D., Hutchins, N., Schultz, M. P., and Flack, K. A., 2021, “Predicting the Drag of Rough Surfaces,” *Annual Review of Fluid Mechanics*, Vol. 53, pp. 439–471.

Colebrook, C. F., and White, C. M., 1937, “Experiments with Fluid Friction in Roughened Pipes,” *Proceedings of the Royal Society A*, Vol. 161, pp. 367–381.

De Maio, M., Latini, B., Nasuti, F., and Pirozzoli, S., 2023, “Direct Numerical Simulation of Turbulent Flow in Pipes with Realistic Large Roughness at the Wall,” *Journal of Fluid Mechanics*, Vol. 974, A40, pp. 1–37.

De Marchis, M., Saccone, D., Milici, B., and Napoli, E., 2020, “Large-Eddy Simulations of Rough Turbulent Channel Flows Bounded by Irregular Roughness,” *Flow, Turbulence and Combustion*, Vol. 105, pp. 627–648.

Flack, K. A., and Schultz, M. P., 2010, “Review of Hydraulic Roughness Scales in the Fully Rough Regime,” *Journal of Fluids Engineering*, Vol. 132, No. 4, pp. 041203–041210.

Flack, K. A., and Schultz, M. P., 2014, “Roughness Effects on Wall-Bounded Turbulent Flows,” *Physics of Fluids*, Vol. 26, No. 10.

Flack, K. A., Schultz, M. P., and Barros, J. M., 2020, “Skin-Friction Measurements of Systematically-Varied Roughness,” *Flow, Turbulence and Combustion*, Vol. 104, pp. 317–329.

Forooghi, P., Weidenlener, A., Magagnato, F., Böhm, B., Kubach, H., Koch, T., and Frohnapfel, B., 2018, “DNS of Momentum and Heat Transfer over Rough Surfaces Based on Realistic Combustion Chamber Deposit Geometries,” *International Journal of Heat and Fluid Flow*, Vol. 69, pp. 83–94.

Garg, H., Wang, L., Sahut, G., and Fureby, C., 2023, “Large Eddy Simulations of Fully Developed Turbulent Flows over Additively Manufactured Rough Surfaces,” *Physics of Fluids*, Vol. 35, 045145, pp. 1–17.

Jouybari, M. A., Yuan, J., Brereton, G. J., and Murillo, M. S., 2021, “Data-Driven Prediction of the Equivalent Sand-

Grain Height in Rough-Wall Turbulent Flows," Journal of Fluid Mechanics, Vol. 912, A8.

Kuwata, Y., and Kawaguchi, Y., 2019, "Direct Numerical Simulation of Turbulence over Systematically Varied Irregular Rough Surfaces," *Journal of Fluid Mechanics*, Vol. 862, pp. 781–815.

Ma, G. Z., Xu, C. X., Sung, H. J., and Huang, W. X., 2022, "Scaling of Rough-Wall Turbulence in a Transitionally Rough Regime," *Physics of Fluids*, Vol. 34, No. 3.

Moody, L. F., 1944, "Friction Factors for Pipe Flow," *Transactions of the ASME*, Vol. 66, pp. 671–678.

Napoli, E., Armenio, V., and De Marchis, M., 2008, "The Effect of the Slope of Irregularly Distributed Roughness Elements on Turbulent Wall-Bounded Flows," *Journal of Fluid Mechanics*, Vol. 613, pp. 385–394.

Nikuradse, J., 1933, "Laws of Flow in Rough Pipes," *VDI-Forschungsheft*, 361 (English translation NACA-TM-1292, 1950).

Sarakinis, S., and Busse, A., 2022, "Investigation of Rough-Wall Turbulence over Barnacle Roughness with Increasing Solidity Using Direct Numerical Simulations," *Physical Review Fluids*, Vol. 7, No. 6, 064602.

Schlichting, H., 1936, "Experimentelle Untersuchungen zum Rauhigkeitsproblem," *Ingenieur-Archiv*, Vol. 7, No. 1, pp. 1–34.

Yang, J., Stroh, A., Chung, D., and Forooghi, P., 2022, "Direct Numerical Simulation-Based Characterization of Pseudo-Random Roughness in Minimal Channels," *Journal of Fluid Mechanics*, Vol. 941, A47, pp. 1–31.

Yuan, J., and Piomelli, U., 2014, "Estimation and Prediction of the Roughness Function on Realistic Surfaces," *Journal of Turbulence*, Vol. 15, No. 6, pp. 350–365.